coatings

MDPI

Article

One-Step Method for Preparing Dispersive Tea Polyphenol/Graphene Nanosheets Enhanced with Anticorrosion Performance

Youwei Guo [1], Guoqing Xiao [1,*], Wei Zhang [2], Nange Zhang [3], Chunling Chen [1], Yi Fan [4], Hongjie Li [1], Xuewei Liu [5] and Yi He [1,*]

1 College of Chemistry and Chemical Engineering, Southwest Petroleum University, Chengdu 610500, China; 201721000270@stu.swpu.edu.cn (Y.G.); 13541694312@163.com (C.C.); 201721000276@stu.swpu.edu.cn (H.L.)
2 Changqing Oilfield No. 3 Oil Harvesting Factory, Chongqing 750006, China; 18609204481@163.com
3 Research Institute of Natural Gas Technology, PetroChina Southwest Oil and Gasfield Company, Chengdu 610051, China; zhang_ng@petrochina.com.cn
4 Chengdu Graphene Application Institute of Industrial Technology, Chengdu 611130, China; tankvan5@gmail.com
5 Research Institute of Petroleum Engineering, PetroChina Dagang Oilfield Company, Tianjin 300280, China; dg_liuxwei@petrochina.com.cn
* Correspondence: gqxiao68@sina.com (G.X.); chemheyi@swpu.edu.cn (Y.H.)

Received: 7 October 2019; Accepted: 31 October 2019; Published: 5 November 2019

Abstract: Water-dispersible and anticorrosion nanocomposites have attracted extensive attention. In this study, tea polyphenol (TP)/graphene (GE) was fabricated with a one-step route. The preparation and modification of graphene nanosheets was carried out by graphene employing tea polyphenols as reduction and functionalization reagents. Our study adopted a nontoxic reductant without an extra functionalization reagent. This method is convenient, inexpensive, and environmentally friendly. The final functionalized graphene nanosheets had a single-layer structure. For evaluating performance, Raman spectroscopy was adapted for evaluating π–π interactions between TP and graphene. Elemental and structural composition was analyzed using X-ray diffraction (XRD) and X-ray photoelectron spectroscopy (XPS). Sample morphology was characterized by scanning electron microscopy (SEM) and transmission electron microscopy (TEM). Results indicated that the TP could effectively augment the dispersive performance of graphene in the solution. The durable anticorrosion capacity of the epoxy matrix noticeably increased after adding the appropriate amount of tea polyphenols–graphene (TPG) (0.3 wt.%). Electrochemical impedance spectroscopy (EIS) studies showed that the impedance of artificial defects was enhanced. The anticorrosion property was attributed to the uniform dispersion of graphene by adding TP.

Keywords: graphene (GE); tea polyphenols (TP); one-step route; nontoxic; TP/GE/epoxy nanocomposites; anticorrosion

1. Introduction

Graphene is a novel material that has a single layer of carbon atoms. It has been used extensively in various technological applications [1] that employ a variety of complex methods to adjust to each circumstance. Graphene is considered to be a promising nanomaterial for the prevention of corrosion [2] because of its excellent chemical-stability, high specific-surface-area, and dominant-barrier properties. Up until now, the anticorrosion performance of metallized materials could be significantly increased with the reduction of defects and layers of graphene, which is supported by several reports [3,4]. For instance, Mogera et al. reported a simple method to create a protective layer of graphene on

the surface of an Ni substrate [5]; moreover, corrosion potential clearly increased and corrosion current density was conspicuously diminished compared with that of a naked substrate. Prasai et al. prepared a graphene layer on a Cu substrate via the chemical-vapor deposition method and observed that the corrosion medium was effectively impeded by the graphene coating [6]. Ersan et al. researched the corrosive-protective mechanism of graphene [7]. The mechanism indicated that the idiosyncratic structure of graphene was the main feature that protected the substrate from penetration by corrosive media. However, the sustainable period of graphene may be reduced because of galvanic corrosion [1], even though studies demonstrated the superiority of graphene in corrosion protection [8,9]. Alternatively, to provide a better protective method, mixing the polymer matrix with graphene to form coatings in epoxy resin [10–12] is advantageous because the composite mixture includes graphene's outstanding barrier performance without the formation of an organic coating. Meanwhile, other attempts have been made to modify the surface of the coating through a range of different types of processing, including electrospinning [13,14], self-assembly [15], sol-gel methods [16,17], and femtosecond laser processing [18]. However, potential interlayer π–π interactions that are imposed on stacking between contiguous graphene nanosheets may result in low solubility of the solution [19]. Currently, functionalized graphene is modified via various chemical reactions and interactions, such as covalent and noncovalent modification [20], π–π stacking, and van der Waals or hydrogen bonding [21]. However, the surface functionalization of graphene by using organic agents suffers from limited expandability and environmental problems. Moreover, adopting functionalization reagents could reduce the effectiveness of graphene and impede practical applications. By comparison with covalent chemical treatment [22,23], noncovalent physical treatment was a more appropriate method because it maintains the structural integrity, water dispersibility, and simple preparation of graphene. For example, Wu et al. employed π–π interactions by combining polypyrrole and graphene to obtain an excellent dispersive solution of graphene [24]. Additionally, the corrosion rate of the metal substrate was effectively reduced by coating it with the hybrid composite [25]. Chen et al. used interactions between MoS_2 and graphene to decrease the agglomeration of graphene in the solution and discovered that the defensive ability of the prepared coating was enhanced due to excellent dispersion [26]. Hence, simultaneous reduction and functionalization is an optimal strategy for the preparation of graphene. However, the key point of durable preparation through noncovalent modification of well-dispersed graphene is still a challenge [27,28].

In order to solve the problems mentioned above, we present a method for preparing graphene with improved durability and surface functionalization via a one-step process. Tea polyphenols (TP) were simultaneously used as functionalization reagents, dispersants, and reductants [29,30]. These materials have outstanding water dispersibility and further improved the anticorrosion property of the coating. TP have a great deal of water-soluble polyphenols [29], have low toxicity, and are biodegradable due to including epicatechin (EC), epicatechin gallate (ECG), and epigallocatechin (EGC) or epigallocatechin gallate (EGCG), except for in studies on antioxidant performance [31]. Tea polyphenols have been employed as capping and reducing agents to combine with precious-metal nanoparticles [30]. On the other hand, it has already been proven that hydrothermal treatment reduces graphene oxide (GO) to reduced graphene oxide (rGO) [32,33]. In view of its antioxidant abilities, water solubility, structural characteristics, and other applications in the affordable synthesis of graphene nanosheets, tea polyphenols that are used for the functionalization of graphene nanosheets impart outstanding water dispersibility and excellent corrosion-medium resistance performance. Next, we used X-ray diffraction (XRD), Raman spectroscopy, X-ray photoelectron spectroscopy (XPS), scanning electron microscopy (SEM), and transmission electron microscopy (TEM) to characterize the structure, composition, and morphology of noncovalently functionalized graphene nanosheets. We also used electrochemical impedance spectroscopy (EIS) to investigate the anticorrosion ability of the coating in sodium chloride solution. Moreover, results indicated that graphene nanosheets that are synthesized via this method have satisfactory water-dispersibility properties by avoiding stacking, and excellent corrosion resistance in hostile environments.

2. Materials and Methods

2.1. Materials

Graphene oxide powder (purity ≥ 99.5%) and tea polyphenols ($C_{22}H_{18}O_{11}$, purity > 99%, molecular weight: 458.372) were purchased from Fuzhou Corona Science and Technology Co., Ltd. (Fuzhou, China) The other chemical agents were analytical-grade without further purification. Deionized water with a resistance of 18.0 MW was collected using the water-purification system of UPC-III and was used to composite all the aqueous solutions.

2.2. Synthesis of TP/GE (Graphene) Nanocomposites

In the beginning of the experiments (Figure 1), graphene oxide powder (10 mg) was mixed into deionized water (20 mL). Then, the processes of stirring and sonication were performed to obtain the dispersive solution. Afterwards, the TP powder (60 mg) was added into the deionized water (20 mL) and combined with the GO solution (0.5 mg·mL^{-1}, 20 mL) through adequate stirring until the solution was uniform. After 20 min of ultrasonic treatment, the prepared solution was transferred to a Teflon-lined stainless-steel autoclave (50 mL), poured into the hydrothermal reactor, and maintained at 90 °C for 8 h. Final products were obtained by washing 3 times with deionized water and freeze-drying (−50 °C, 72 h) for further characterization.

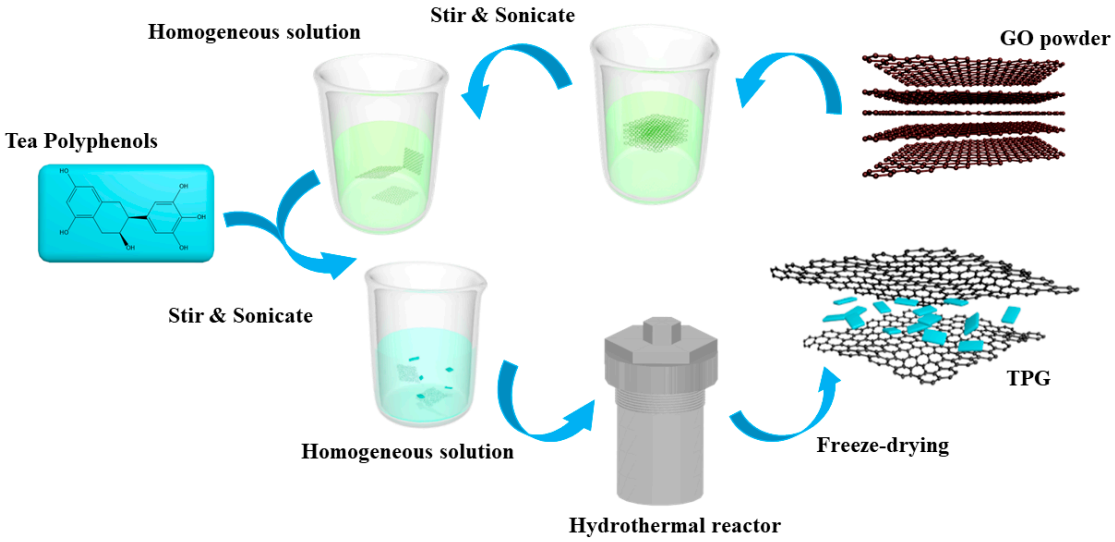

Figure 1. Simple synthetic schematic of tea polyphenol (TP)/graphene (GE).

2.3. Composite-Coating Manufacture

The obtained TP/GE powder was added into epoxy (3.34 g) followed by the corresponding curing agent (1.67 g). This mixture was stirred for 10 min to ensure complete compatibility. The tea polyphenol–graphene (TPG)/epoxy mixture was used on preprocessed Q235 steel (50 mm × 10 mm × 10 mm) with a sandblasting machine (Yuxin Machinery Equipment Co. Ltd., GuangZhou, China). Surface cleanliness was at a Sa2.5 level with an approximate thickness of 150 ± 4 μm. In addition, the pure epoxy matrix was coated as the control group for comparison with 0.1 wt.%, 0.3 wt.%, and 0.6 wt.%.

2.4. Material Characterization

Structure and phase analysis of the composite materials were performed using XRD (PANalytical, Shanghai, China); the emission source of the X-ray was designed as a copper Kα (wavelength λ = 0.154 nm), with a tube voltage of 40 kV and a slit of approximately 0.15 mm. The tube flow was 100 mA, the emission slit was 1/6°, and the anti-scattering slit was 1/6°. The scanning rate of the samples was 6°/min, the scanning range corresponded to 5°–90°, and the scan length was 0.02°. The Raman spectra

of the samples were collected (at room temperature) with a Renishaw InVia confocal Raman microscope (Wotton-under-Edge, UK). XPS analysis for characterizing chemical bonds was performed with a KRATOS XSAM 800 (Monochromatic Al Kα; HV = 1486.6 eV, KRATOS XSAM 800, Manchester, UK) with a power of 150 W and combination calibration using C 1*s* 284.8. For the Atomic Force Microscope (AFM), the surface topography of the samples was examined at room temperature on an SPI 4000 Probe Station and SPA-400 SPM Unit (Seiko Instruments Inc., Chiba, Japan) via a tapping mode. The TEM and desired selected-area electron diffraction (SAED) were obtained from functionalized graphene sheets that were freeze-dried with JEM-2100F, Japan Electron Optics Laboratory Co., Ltd. (Tokyo, Japan) Morphology analysis of the TP/GE nanomaterials was carried out with an SEM (FE-SEM; acceleration voltage was 5–30 kV).

2.5. Electrochemical Experiment

The CorrTest CS350 system (CS350, Corrtest instruments Corp. Ltd., Wuhan, China) was used for polarization analysis and to obtain electrochemical impedance spectra at room temperature with a 3.5 wt.% NaCl solution. The reference electrode consisted of a 3-electrode cell with a saturated calomel electrode (SCE) and a platinum wire as a counter electrode. The working electrode was adopted from an exposed sample region of 1 cm^2. Polarization parameters were measured by scanning from 200 mV SCE under open-circuit potential to 250 mV SCE at a rate of 1 mV s^{-1}. Corrosion potential (Ecorr) and corrosion current density (Icorr) were fitted from the crossing of the anodic and cathodic Tafel curves using the Tafel extrapolation method. Working electrodes were immersed in the solution for 30 min before the start of the tests.

3. Results and Discussion

3.1. Structural Analysis of the TP/GE Composite Material

XRD and Raman spectroscopy were used to structurally characterize the functionalized graphene nanosheets. Reactive changes of the structural exfoliated graphene were obtained by XRD. Figure 2a exhibits the XRD patterns of GO, reduced graphene oxide (marked as GE), and TPG gained by the continuous reaction of GE with TP. Due to the introduction of oxygenated functional groups, the XRD GO profile showed a strong single reflection at 2θ = 10.4°, which corresponded to an increased interlayer d_{001} spacing of 0.86 nm, which was larger compared to that of graphite (0.34 nm), and the XRD GE profile presented a prominent single reflection at 2θ = 25.8°, which conformed to traditional industrial graphene that has an interlayer d_{002} spacing of 0.34 nm. For comparison, the XRD profile of TPG, which was prepared from TPG dispersion, showed low-angle reflection at 2θ = 6.4° that resembled enlarged interlayer spacing (d_{100}) of 1.4 nm, indicating a regular lamellar nanostructure including a stacked arrangement of surface-functionalization molecules inserted with graphene nanosheets. Another highly broadened peak at 2θ = 26.3° (d_{002} = 0.34 nm) was in accordance with the d_{002} of the initial graphite; the pure graphene nanosheets without further surface treatment indicated the chaotic stacking nature of tiny-sized graphene nanosheets without functional oxygen groups [34]. To further confirm the degree of graphitization, Raman spectroscopic studies were conducted. The Raman spectrum characterization of TPG (Figure 2b) in the solvent (532 nm laser excitation) is depicted by two highlighted bands at 1345 and 1589 cm^{-1}, corresponding with the G and D modes. The G band, dated from the zone-center E2g mode, was consistent with well-organized sp2-bonded carbon atoms and the D band was attributed to the few defects, edge wrinkles, and disordered carbon atoms [35]. The disordered D band was outstanding compared to the ordered G band. The ratio of ID/IG reached 1.07 for TPG, which indicated partial recovery of the graphene structure and the limited mean size of the sp2 bond carbon fields; this size is ascribed to the increased smaller graphitic fields that are formed by the reduction process. The consequence is similar to previous reports of chemically reduced graphene.

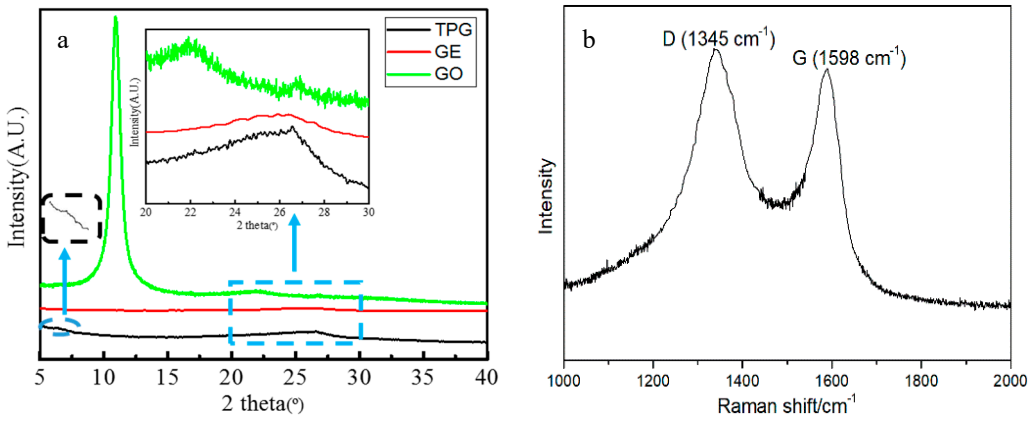

Figure 2. (**a**) X-ray diffraction (XRD) spectrum of TP/GE powder and GE; (**b**) Raman spectrum of tea polyphenols–graphene (TPG) solution.

The high-resolution C 1*s* spectra of TP/GE and GE were detected using XPS, and spectrum decomposition was performed using the XPS PEAK 41 program with Gaussian functions after subtraction of a Shirley background, as shown in Figure 3. The C 1*s* XPS spectrum of GE (Figure 3a) by fitting showed that a large number of peaks were ascribed to carbon atoms in different functional groups: C–C (284.6 eV), carbon atoms in the C–H bond (285.7 eV), and the C–O bond (287.2 eV). The ingredient peak at around 291.0 eV was comparable to π–π* interactions [29], which are characteristic of aromatic or conjugated systems. The C 1*s* XPS spectrum of TPG (Figure 3b) also exhibited corresponding characteristics, indicating some of the same oxygen peaks of functionalized molecules, because peak intensities were much larger than those of GE. Obviously, TP and their oxidization products were attributed to the C–O bond (285.6 eV) and the COOH bond (288.3 eV), respectively. According to the above characterization, in this experiment, reduction was due to the combined effect of hydrothermal treatment and TP [36].

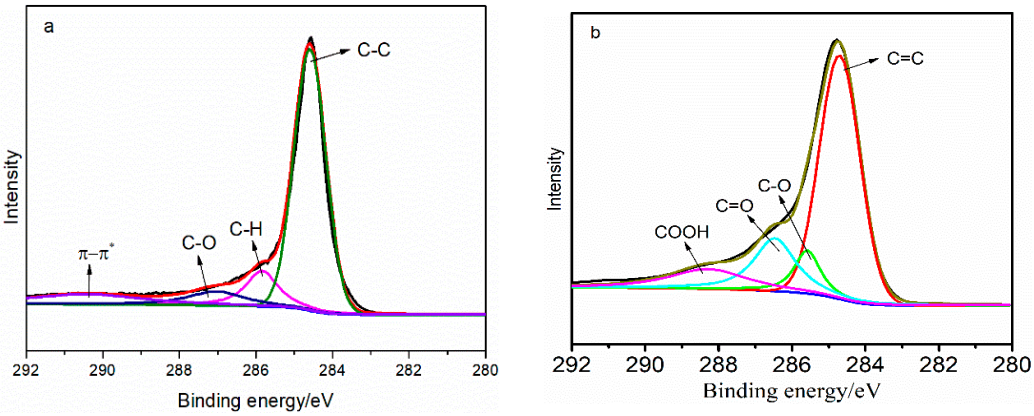

Figure 3. X-ray photoelectron spectroscopy (XPS) tests on high-resolution scans of C 1*s* spectra of (**a**) GE and (**b**) TPG.

3.2. Morphology Analysis

SEM and TEM were adopted for analyzing the internal morphology of TPG nanosheets. The SEM images of the dispersed TPG nanosheets (Figure 4a,b), which were collected by freeze-drying (ratio between TP and graphene in the obtained product was 6:1), were successive over a large area with some apparent accumulation with the product of tea polyphenols and a few apparent wrinkles. According to the TEM image (Figure 4c), an important feature of TPG was observed: ultrathin and single-layer nanosheet along with incidental folds [16], cracks, and rolled edges, possibly caused by reaction sites in the chemical process. These features corresponded with the SAED pattern (TPG nanosheet)

shown in Figure 4d, and an area of TPG is outlined with a black square in Figure 4d. The explicitly identified sixfold symmetry diffraction pattern distinguished the crystalline structure of the TPG. Compared with the outer {2110}c peaks, the intensity of the inner {1100} peaks of the diffraction pattern were more intense, which confirmed the production of monolayer TPG from the reaction of GE with TPG. In Figure 5, AFM (tapping mode) was used to identify the features of single-layer GE and TPG nanosheets. Cross-section analyses of GE and TPG are shown in Figure 5; the powders of GE and TPG included a large number of single-layer flakes. For the AFM image, GE thickness was around 3 nm, which measured up to the form of commercial graphene. By comparison with TPG, the display of a clear lamellar structure with flake thickness reaching 4.3–5.2 nm indicated excellent dispersion and supports that the TP was successfully combined with GE [37].

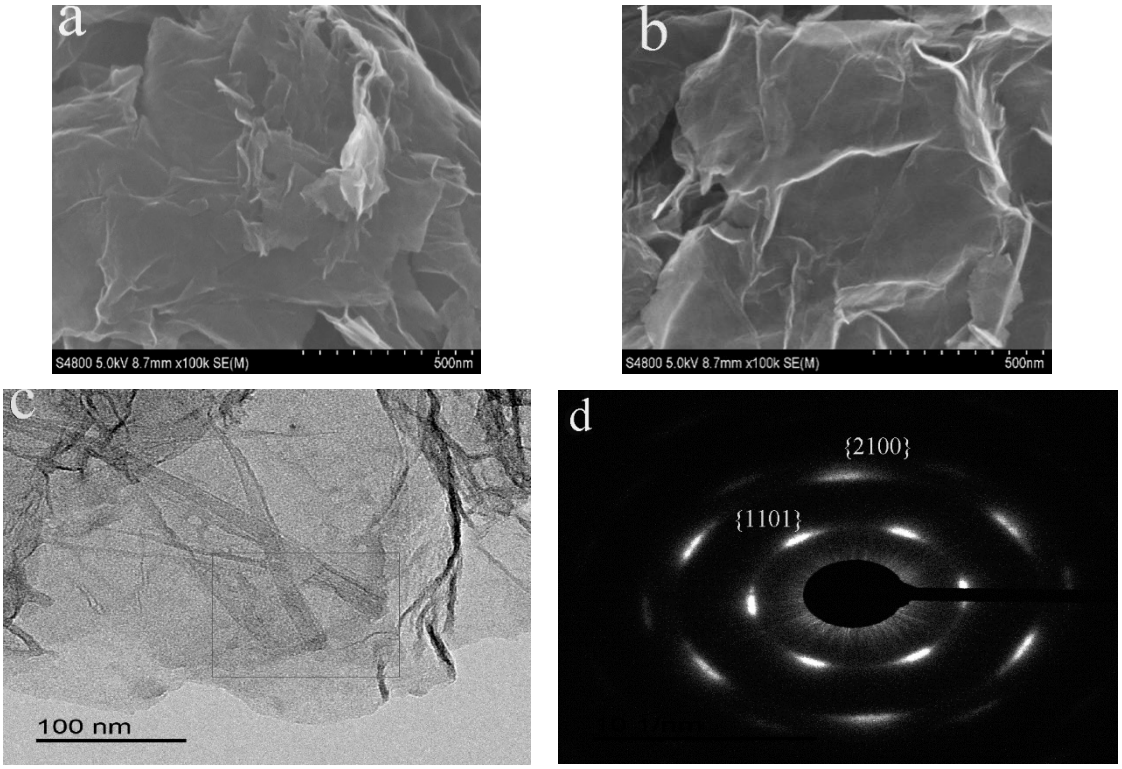

Figure 4. (**a**,**b**) Scanning electron microscopy (SEM) image of TPG. (**c**) Transmission electron microscopy (TEM) image of TPG. (**d**) Corresponding selected-area electron diffraction (SAED) of TPG nanosheet area outlined with a black rectangle in Figure 4c.

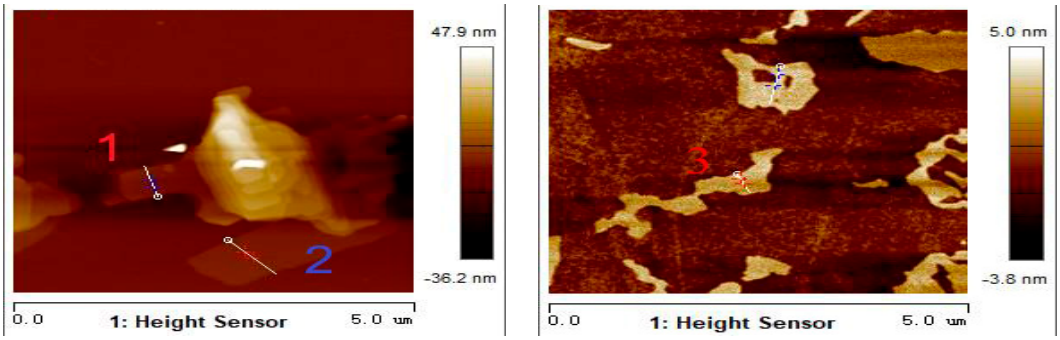

(**a**) (**b**)

Figure 5. *Cont.*

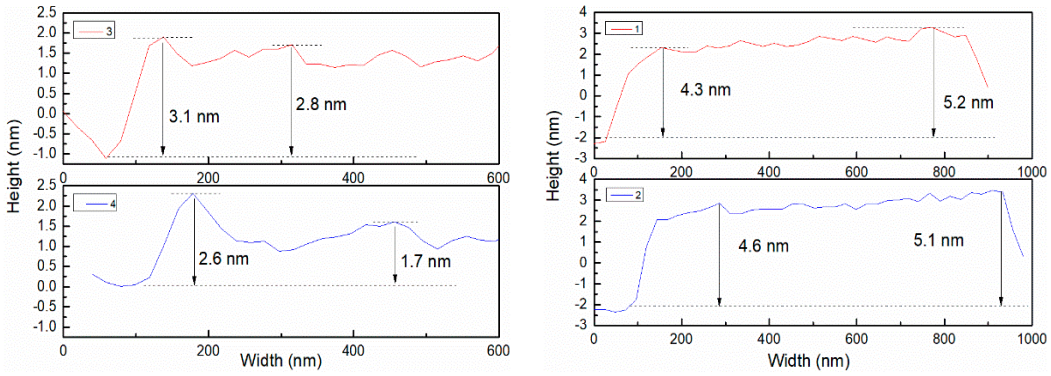

Figure 5. Tapping-mode atomic force microscope (AFM) images: (**a**) graphene, (**b**) nanocomposite TPG and corresponding height profiles of (**c**) GE and (**d**) TPG.

3.3. Anticorrosive Performance

The performance of the anticorrosion coating was confirmed by electrochemical-impedance assessment. Samples were immersed in an NaCl solution (3.5 wt.%) before the test in order to obtain a steady open-circuit electrode. The impedance spectra of EP, TP/GE (0.1 wt.%), TP/GE (0.3 wt.%), and TP/GE (0.6 wt.%) are presented in Figure 6. The impedance arc showed that TP/GE (0.3 wt.%) was wider than those of TP/GE (0.1 wt.%), TP/GE (0.6 wt.%), and pure EP, which indicated that the largest impedance was that of TP/GE (0.3 wt.%). The Bode diagrams of coating clarified that all the tested coatings exhibited the one-time constant and suggested that the coating was in the initial immersion stage. The impedance of EP, TP/GE (0.1 wt.%), and TP/GE (0.6 wt.%) was sharply decreased compared to TP/GE (0.3 wt.%) due to increasing immersion time to 400 h (Figure 7). Bode diagrams showing the two-time constant and Warburg impedance arc indicated that the corrosion medium penetrated the anticorrosion interface [37]. In addition, the equivalent electrical-circuit model is presented in Figure 8a. Symbols Rs, CPE, and R1/R2 denote solution resistance, capacitance, and resistance of the nanocomposite coating, respectively. In the testing stage, the rates of corrosion from corrosive solutions passing through pores of coating are far less when compared with the corrosion rates of corrosive products during the interface contact of the coating and metal matrix [37]. The equivalent electrical-circuit model is shown in Figure 8b, where R3, C, and CPE are microporous resistance, double-layer capacitance, and constant-phase element, respectively [38,39]. Characterization of anticorrosion performance illustrated that adding TP/GE (0.3 wt.%) could increase the impenetrability trait and corrosion resistance of the coating.

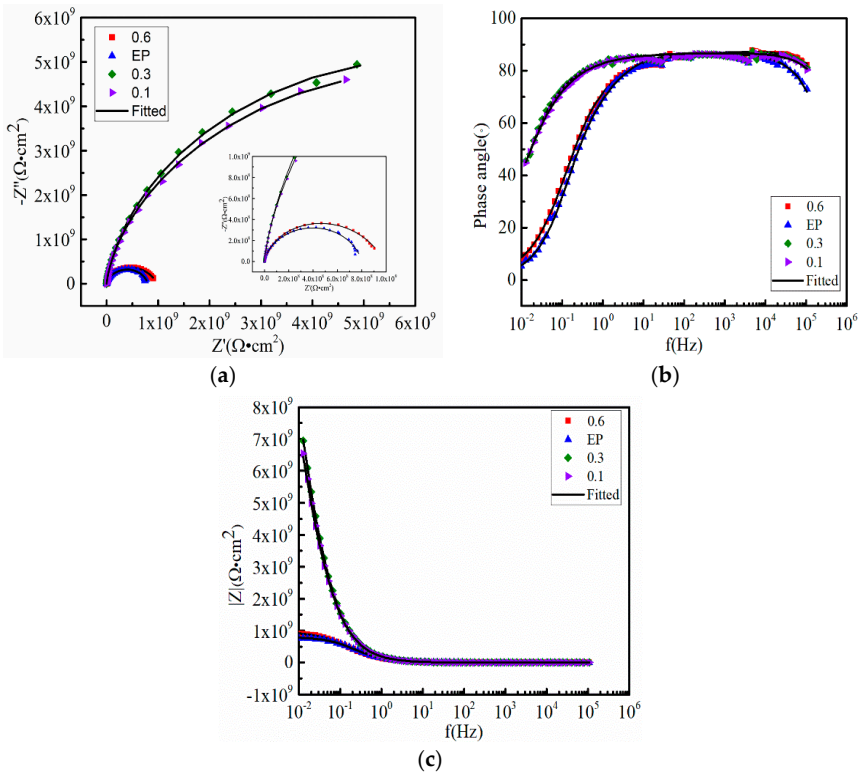

Figure 6. Nyquist and Bode diagrams of composite coatings coated with different ration of TPG (**a**–**c**) after immersion for 120 h in 3.5% NaCl solution.

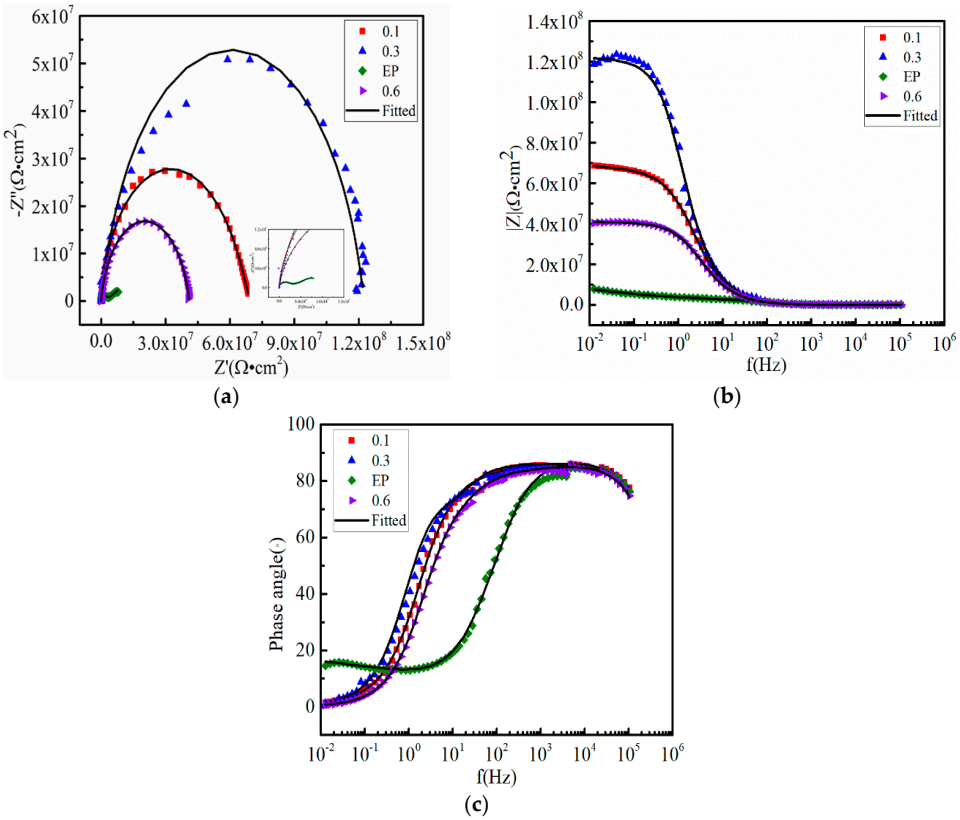

Figure 7. Nyquist and Bode diagrams of composite coatings coated with different ration of TPG (**a**–**c**) after immersion for 400 h in 3.5% NaCl solution.

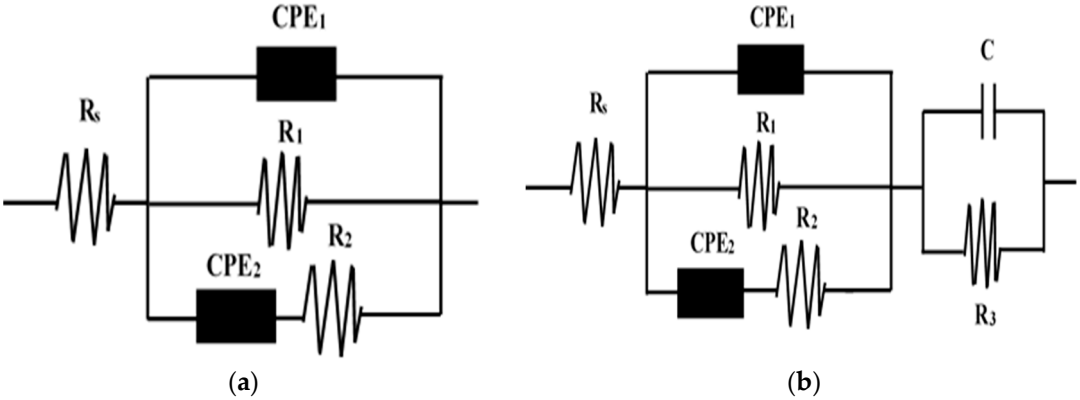

Figure 8. Equivalent electrical-circuit model: (**a**) the original state of corrosion in 3.5% NaCl solution, (**b**) corrosion state after a certain period of time in 3.5% NaCl solution.

3.4. Polarization-Curve Test

The polarization curves of EP and the different ratio of EP/TPG was confirmed (Figure 9) with exposure to an NaCl solution (3.5 wt.%) for 30 days; the corrosion parameter of the hybrid coating and EP is shown in Table 1. The corrosion potential is denoted by Ecorr, and the anodic (βa), corrosion-current-density (icorr), and cathodic (βc) slopes were confirmed by Tafel plots. It was verified that the pure EP coating showed negative Ecorr (−0.65 V) in the 30 days of testing due to the effect of the corrosion agent at the interface. EP/TPG (0.3 wt.%) presented satisfying performance of Ecorr (−0.589 V), which was lower than that of EP/TPG (0.1 wt.%) and EP/TPG (0.6 wt.%). In addition, the icorr of EP/TPG (0.3 wt.%) was diminished, which indicated outstanding protective ability that was due to excellent dispersion and barrier.

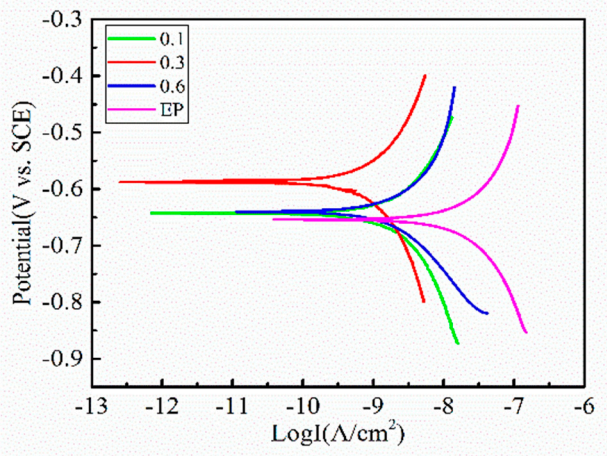

Figure 9. Polarization plots of pure epoxy and nanocomposite TPG.

Table 1. Corrosion parameters of the polarization curve of the composite coating.

System	Ecorr (V)	βa (mV)	βc (mV)	Icorr (A/cm^2)	Corrosion Rate (mm/a)
Epoxy	−0.65305	154.18	156.02	1.5896×10^{-8}	1.8648×10^{-4}
TP/GE (0.1 wt.%)	−0.64122	110.24	131.21	1.2515×10^{-9}	1.4682×10^{-5}
TP/GE (0.3 wt.%)	−0.58949	148.15	146.83	6.1457×10^{-10}	7.2096×10^{-6}
TP/GE (0.6 wt.%)	−0.64003	362.35	230.53	4.6053×10^{-9}	5.4026×10^{-5}

3.5. Spray Test for the Hybrid Coating

The corrosive surface of TPG and GE, which was investigated by using a spray test after long-term immersion (100 and 400 h) in an NaCl solution (5 wt.%), is presented in Figure 10. Small amounts of corrosion products located in the scratches of the samples could be observed after 100 h exposure in EP, 0.1% TPG/EP, and 0.6% TPG/EP. With the increase of immersion time (400 h), more corrosion products accumulated around the scratches. Corrosive agents permeated the coating interface, which disturbed anticorrosion performance due to aggressive ions penetrating the micropores in the coating system. However, by incorporating 0.3% TPG/GE, improved anticorrosion performance was observed, as shown in Figure 10c,c′; 0.3% TPG/GE had the fewest corrosion products and bubbles. It was indicated that 0.3% TPG/EP had a satisfactory barrier against the corrosive impact on the interface.

Figure 10. Corrosive-surface images of the spray test exposed for 100 and 400 h in 5 wt.% NaCl solution. (**a**,**a′**) Pure EP coating; (**b**,**b′**) 0.1%, (**c**,**c′**) 0.3%, and (**d**,**d′**) 0.6% EP/TPG.

4. Conclusions

A simple, sustainable method for preparing a TPG anticorrosion coating was discussed. It showed great GE dispersion and was enhanced by TP as a functional reagent, which can avoid issues such as toxic reductants, complicated preparation methods, and graphene accumulation in the solution. In addition, TPG nanosheets have large surfaces and, combined with epoxy, could enhance the coating barrier in terms of electrochemistry tests. EP/TPG 0.3 wt.% exhibited superior performance compared

with the others in EIS due to the significant prevention of aggressive media permeating the coating. This ecofriendly method for dispersing GE, with applications in anticorrosion, merits further study.

Author Contributions: Conceptualization, Y.G. and Y.F.; data curation, H.L.; investigation, C.C.; project administration, N.Z., W.Z. and X.L.; funding acquisition, Y.H.; supervision, G.X.; writing-review and editing, Y.G.

Funding: This research was funded by The National Natural Science Foundation of China (No. 51774245) and the Applied Basic Research Program of the Science and Technology Department of Sichuan Province (No. 2018JY0517).

Acknowledgments: The authors would like to acknowledge the College of chemistry and Chemical engineering of Southwest petroleum university for their supporting devices.

Conflicts of Interest: The authors declare no conflict of interest.

References

1. Cui, G.; Bi, Z.; Zhang, R.; Liu, J.; Yu, X.; Li, Z. A comprehensive review on graphene-based anti-corrosive coatings. *Chem. Eng. J.* **2019**, *373*, 104–121. [CrossRef]
2. Bohm, S. Graphene against corrosion. *Nat. Nanotechnol.* **2014**, *9*, 741–742. [CrossRef] [PubMed]
3. Koo, H.Y.; Lee, H.-J.; Go, H.-A.; Lee, Y.B.; Bae, T.S.; Kim, J.K.; Choi, W.S. Graphene-based multifunctional iron oxide nanosheets with tunable properties. *Chem. Eur. J.* **2011**, *17*, 1214–1219. [CrossRef]
4. Parhizkar, N.; Shahrabi, T.; Ramezanzadeh, B. A new approach for enhancement of the corrosion protection properties and interfacial adhesion bonds between the epoxy coating and steel substrate through surface treatment by covalently modified amino functionalized graphene oxide film. *Corros. Sci.* **2017**, *123*, 55–75. [CrossRef]
5. Mogera, U.; Kurra, N.; Radhakrishnan, D.; Narayana, C.; Kulkarni, G.U. Low cost, rapid synthesis of graphene on Ni: An efficient barrier for corrosion and thermal oxidation. *Carbon* **2014**, *78*, 384–391. [CrossRef]
6. Prasai, K.; Chen, G.; Drabold, D.A. Amorphous to amorphous insulator-metal transition in $GeSe_3$:Ag glasses. *Phys. Rev. Mater.* **2017**, *1*, 015603. [CrossRef]
7. Ersan, G.; Apul, O.G.; Perreault, F.; Karanfil, T. Adsorption of organic contaminants by graphene nanosheets: A review. *Water Res.* **2017**, *126*, 385–398. [CrossRef]
8. Chen, C.; He, Y.; Xiao, G.; Wu, Y.; He, Z.; Zhong, F. Zirconia doped in carbon fiber by electrospinning method and improve the mechanical properties and corrosion resistance of epoxy. *Prog. Org. Coat.* **2018**, *125*, 420–431. [CrossRef]
9. Guo, S.; Dong, S. Graphene nanosheet: Synthesis, molecular engineering, thin film, hybrids, and energy and analytical applications. *Chem. Soc. Rev.* **2011**, *40*, 2644–2672. [CrossRef]
10. Chen, B.; Ni, B.-J.; Liu, W.-T.; Ye, Q.-Y.; Liu, S.-Y.; Zhang, H.-X.; Yoon, K.-B. Mechanical properties of epoxy nanocomposites filled with melamine functionalized molybdenum disulfide. *RSC Adv.* **2018**, *8*, 20450–20455. [CrossRef]
11. Eksik, O.; Gao, J.; Shojaee, S.A.; Thomas, A.; Chow, P.; Bartolucci, S.F.; Lucca, D.A.; Koratkar, N. Epoxy nanocomposites with two-dimensional transition metal dichalcogenide additives. *ACS Nano* **2014**, *8*, 5282–5289. [CrossRef]
12. Ghanbari, A.; Attar, M.M. A study on the anticorrosion performance of epoxy nanocomposite coatings containing epoxy-silane treated nano-silica on mild steel substrate. *J. Ind. Eng. Chem.* **2015**, *23*, 145–153. [CrossRef]
13. An, A.K.; Guo, J.; Lee, E.-J.; Jeong, S.; Zhao, Y.; Wang, Z.; Leiknes, T. PDMS/PVDF hybrid electrospun membrane with superhydrophobic property and drop impact dynamics for dyeing wastewater treatment using membrane distillation. *J. Membr. Sci.* **2017**, *525*, 57–67. [CrossRef]
14. Gong, G.; Gao, K.; Wu, J.; Sun, N.; Zhou, C.; Zhao, Y.; Jiang, L. A highly durable silica/polyimide superhydrophobic nanocomposite film with excellent thermal stability and abrasion-resistant performance. *J. Mater. Chem. A* **2015**, *3*, 713–718. [CrossRef]
15. Mao, J.; Ge, M.; Huang, J.; Lai, Y.; Lin, C.; Zhang, K.; Meng, K.; Tang, Y. Constructing multifunctional MOF@rGO hydro-/aerogels by the self-assembly process for customized water remediation. *J. Mater. Chem. A* **2017**, *5*, 11873–11881. [CrossRef]
16. Nine, M.J.; Cole, M.A.; Tran, D.N.H.; Losic, D. Graphene: A multipurpose material for protective coatings. *J. Mater. Chem. A* **2015**, *3*, 12580–12602. [CrossRef]

17. Zhang, H.; Hou, C.; Song, L.; Ma, Y.; Ali, Z.; Gu, J.; Zhang, B.; Zhang, H.; Zhang, Q. A stable 3D sol-gel network with dangling fluoroalkyl chains and rapid self-healing ability as a long-lived superhydrophobic fabric coating. *Chem. Eng. J.* **2018**, *334*, 598–610. [CrossRef]
18. Lin, Y.; Han, J.; Cai, M.; Liu, W.; Luo, X.; Zhang, H.; Zhong, M. Durable and robust transparent superhydrophobic glass surfaces fabricated by a femtosecond laser with exceptional water repellency and thermostability. *J. Mater. Chem. A* **2018**, *6*, 9049–9056. [CrossRef]
19. Seo, J.-W.T.; Green, A.A.; Antaris, A.L.; Hersam, M.C. High-concentration aqueous dispersions of graphene using nonionic, biocompatible block copolymers. *J. Phys. Chem. Lett.* **2011**, *2*, 1004–1008. [CrossRef]
20. Shang, W.; Wu, F.; Wen, Y.; He, C.; Zhan, X.; Li, Y. Corrosion resistance and mechanism of graphene oxide composite coatings on magnesium alloy. *Ind. Eng. Chem. Res.* **2018**, *58*, 1200–1211. [CrossRef]
21. Shen, L.; Li, Y.; Zhao, W.; Miao, L.; Xie, W.; Lu, H.; Wang, K. Corrosion protection of graphene-modified zinc-rich epoxy coatings in dilute nacl solution. *ACS Appl. Nano Mater.* **2018**, *2*, 180–190. [CrossRef]
22. Wu, Y.Q.; He, Y.; Chen, C.L.; Li, H.J.; Xia, Y.Q.; Zhou, T.G. MoS_2-CNFs composites to enhance the anticorrosive and mechanical performance of epoxy coating. *Prog. Org. Coat.* **2019**, *129*, 178–186. [CrossRef]
23. Xia, Y.; He, Y.; Chen, C.; Wu, Y.; Chen, J. MoS_2 nanosheets modified SiO_2 to enhance the anticorrosive and mechanical performance of epoxy coating. *Prog. Org. Coat.* **2019**, *132*, 316–327. [CrossRef]
24. Wu, F.; Xie, A.; Sun, M.; Wang, Y.; Wang, M. Reduced graphene oxide (RGO) modified spongelike polypyrrole (PPy) aerogel for excellent electromagnetic absorption. *J. Mater. Chem. A* **2015**, *3*, 14358–14369. [CrossRef]
25. Baux, J.; Causse, N.; Esvan, J.; Delaunay, S.; Tireau, J.; Roy, M.; You, D.; Pebere, N. Impedance analysis of film-forming amines for the corrosion protection of a carbon steel. *Electrochim. Acta* **2018**, *283*, 699–707. [CrossRef]
26. Chen, C.; He, Y.; Xiao, G.; Xia, Y.; Li, H.; He, Z. Two-dimensional hybrid materials: MoS_2-RGO nanocomposites enhanced the barrier properties of epoxy coating. *Appl. Surf. Sci.* **2018**, *444*, 511–521. [CrossRef]
27. Tian, S.; Sun, J.; Yang, S.; He, P.; Wang, G.; Di, Z.; Ding, G.; Xie, X.; Jiang, M. Controllable edge oxidation and bubbling exfoliation enable the fabrication of high quality water dispersible graphene. *Sci. Rep.* **2016**, *6*, 34127. [CrossRef]
28. Zhang, Y.; Zou, Q.; Hsu, H.S.; Raina, S.; Xu, Y.; Kang, J.B.; Chen, J.; Deng, S.; Xu, N.; Kang, W.P. Morphology effect of vertical graphene on the high performance of supercapacitor electrode. *ACS Appl. Mater. Interfaces* **2016**, *8*, 7363–7369. [CrossRef]
29. Song, H.; Hao, L.; Tian, Y.; Wan, X.; Zhang, L.; Lv, Y. Stable and water-dispersible graphene nanosheets: Sustainable preparation, functionalization, and high-performance adsorbents for Pb^{2+}. *ChemPlusChem* **2012**, *77*, 379–386. [CrossRef]
30. Wang, Z.; Xu, C.; Li, X.; Liu, Z. In situ green synthesis of Ag nanoparticles on tea polyphenols-modified graphene and their catalytic reduction activity of 4-nitrophenol. *Colloids Surf. Physicochem. Eng. Asp.* **2015**, *485*, 102–110. [CrossRef]
31. Akhavan, O.; Kalaee, M.; Alavi, Z.S.; Ghiasi, S.M.A.; Esfandiar, A. Increasing the antioxidant activity of green tea polyphenols in the presence of iron for the reduction of graphene oxide. *Carbon* **2012**, *50*, 3015–3025. [CrossRef]
32. Pant, B.; Saud, P.S.; Park, M.; Park, S.J.; Kim, H.Y. General one-pot strategy to prepare Ag-TiO_2 decorated reduced graphene oxide nanocomposites for chemical and biological disinfectant. *J. Alloys Compd.* **2016**, *671*, 51–59. [CrossRef]
33. Pant, B.; Park, M.; Park, S.J.; Kim, H.Y. One-pot synthesis of CdS sensitized TiO_2 decorated reduced graphene oxide nanosheets for the hydrolysis of ammonia-borane and the effective removal of organic pollutant from water. *Ceram. Int.* **2016**, *42*, 15247–15252. [CrossRef]
34. Pant, B.; Pokharel, P.; Tiwari, A.P.; Saud, P.S.; Park, M.; Ghouri, Z.K.; Choi, S.; Park, S.J.; Kim, H.Y. Characterization and antibacterial properties of aminophenol grafted and Ag NPs decorated graphene nanocomposites. *Ceram. Int.* **2015**, *41*, 5656–5662. [CrossRef]
35. Ding, R.; Li, W.; Wang, X.; Gui, T.; Li, B.; Han, P.; Tian, H.; Liu, A.; Wang, X.; Liu, X.; et al. A brief review of corrosion protective films and coatings based on graphene and graphene oxide. *J. Alloys Compd.* **2018**, *764*, 1039–1055. [CrossRef]
36. Zhang, H.; Lv, X.J.; Li, Y.M.; Wang, Y.; Li, J.H. P25-graphene composite as a high performance photocatalyst. *ACS Nano* **2010**, *4*, 380–386. [CrossRef]

37. Cui, M.; Ren, S.; Zhao, H.; Xue, Q.; Wang, L. Polydopamine coated graphene oxide for anticorrosive reinforcement of water-borne epoxy coating. *Chem. Eng. J.* **2018**, *335*, 255–266. [CrossRef]
38. Faure, M.; Billon, F.; Haghiri-Gosnet, A.M.; Tribollet, B.; Deslouis, C.; Pailleret, A.; Gamby, J. Influence of the atomic nitrogen content in amorphous carbon nitride thin films on the modulation of their polarizable interfaces properties. *Electrochim. Acta* **2018**, *280*, 238–247. [CrossRef]
39. Jayaraj, J.; Raj, S.A.; Srinivasan, A.; Ananthakumar, S.; Pillai, U.T.S.; Dhaipule, N.G.K.; Mudali, U.K. Composite magnesium phosphate coatings for improved corrosion resistance of magnesium AZ31 alloy. *Corros. Sci.* **2016**, *113*, 104–115. [CrossRef]